Seismic Reliability Analysis of Energy-dissipation Structures by PDEM-ETDM

Jianhua Xian
Ph.D. Student, School of Civil Engineering and Transportation, South China University of Technology, Guangzhou, China

Cheng Su
Professor, School of Civil Engineering and Transportation & State Key Laboratory of Subtropical Building Science, South China University of Technology, Guangzhou, China
Corresponding author (cvchsu@scut.edu.cn)

ABSTRACT: Energy-dissipation devices have been widely used for improving the performance of civil structures exposed to seismic hazard. In this study, a hybrid approach, which combines the probability density evolution method (PDEM) and the explicit time-domain method (ETDM), is proposed for the seismic reliability analysis of large-scale energy-dissipation structures with uncertain parameters of nonlinear energy-dissipation devices subjected to random seismic excitations. To demonstrate the feasibility of the proposed approach, a dynamic reliability analysis under random seismic excitations is carried out for a suspension bridge with a main span of 1,200 m equipped with 4 nonlinear viscous dampers with uncertain parameters.

1. INTRODUCTION

Passive control using energy-dissipation devices has received considerable attention in recent years and has proven to be a very effective method for enhancing the performance of civil structures exposed to seismic hazard (Soong and Spencer, 2002). In view of the popular use of energy-dissipation devices in real engineering problems, there is a growing need for an effective seismic reliability analysis method of large-scale energy-dissipation structures. On the other hand, the parameters of the energy-dissipation devices might be uncertain to some extent due to the manufacturing errors, and their uncertainties may have a significant impact on the dynamic reliabilities of energy-dissipation structures under seismic excitations. The seismic reliability assessment of large-scale energy-dissipation structures with uncertain parameters of energy-dissipation devices is a more complex problem.

For the first-passage problems, the dynamic reliability evaluation is equivalent to obtaining the peak-response probability density function (PDF). The probability density evolution method (PDEM) is capable of capturing the peak-response PDF of a nonlinear stochastic structure by constructing a virtual random process associated with the peak response (Chen and Li, 2007; Li and Chen, 2009). The seismic failure probability of the structure can then be directly evaluated through the integration of the peak-response PDF over the failure domain. However, hundreds of deterministic nonlinear time-history analyses are embedded in the solution process of PDEM to compute the coefficients involved in the probability density evolution equation, which leads to relatively high computational cost for large-scale engineering structures when conventional numerical integration methods are adopted.

To enhance the efficiency of PDEM, the explicit time-domain method (ETDM) with dimension-reduced explicit iteration scheme, recently proposed for time-history analysis of large-scale nonlinear systems (Su et al., 2018a; Su et al., 2018b), is incorporated into PDEM to

conduct the high-efficient nonlinear dynamic analyses, in which only a small number of degrees of freedom associated with the energy-dissipation devices are considered in the iteration process. To demonstrate the feasibility of the above hybrid approach, the PDEM-ETDM, a dynamic reliability analysis under random seismic excitations is carried out for a suspension bridge with a main span of 1,200 m equipped with 4 nonlinear viscous dampers with uncertain parameters.

2. SEISMIC RELIABILITY ANALYSIS OF ENERGY-DISSIPATION STRUCTURES BY PDEM

2.1. Seismic reliability evaluation of energy-dissipation structures

For an energy-dissipation structure equipped with n_{d} nonlinear energy-dissipation devices with uncertain parameters subjected to random seismic excitations, the nonlinear equation of motion can be expressed as

$$\mathbf{M}\ddot{\mathbf{U}}+\mathbf{C}\dot{\mathbf{U}}+\mathbf{K}\mathbf{U}+\mathbf{L}_{\mathrm{D}}\mathbf{F}_{\mathrm{D}}(\boldsymbol{\Theta},\mathbf{V}_{\mathrm{D}})=-\mathbf{M}\mathbf{E}X(\boldsymbol{\Theta},t) \quad (1)$$

where $\mathbf{M}$, $\mathbf{C}$ and $\mathbf{K}$ are the mass, damping and stiffness matrix of the structure without energy-dissipation devices, respectively; $\mathbf{U}$, $\dot{\mathbf{U}}$ and $\ddot{\mathbf{U}}$ are the time-dependent nodal displacement, velocity and acceleration vector of the energy-dissipation structure, respectively; $\boldsymbol{\Theta}$ is a vector of random parameters involved in the energy-dissipation devices and the seismic excitation; $\mathbf{E}$ is the orientation vector of the seismic excitation; $X(\boldsymbol{\Theta},t)$ is the random seismic excitation; $\mathbf{L}_{\mathrm{D}}$ is the orientation matrix of the nonlinear restoring forces; $\mathbf{V}_{\mathrm{D}}=[\mathbf{U}_{\mathrm{D}}^{\mathrm{T}}\ \dot{\mathbf{U}}_{\mathrm{D}}^{\mathrm{T}}]^{\mathrm{T}}$ with $\mathbf{U}_{\mathrm{D}}$ and $\dot{\mathbf{U}}_{\mathrm{D}}$ being the displacement and velocity vector of the nodes of energy-dissipation devices, respectively; and $\mathbf{F}_{\mathrm{D}}(\boldsymbol{\Theta},\mathbf{V}_{\mathrm{D}})$ is the nonlinear restoring force vector of energy-dissipation devices, which can be written as

$$\mathbf{F}_{\mathrm{D}}(\boldsymbol{\Theta},\mathbf{V}_{\mathrm{D}})=[\,f_1(\boldsymbol{\Theta},t)\ \ f_2(\boldsymbol{\Theta},t)\ \ \cdots\ \ f_{n_{\mathrm{d}}}(\boldsymbol{\Theta},t)]^{\mathrm{T}} \quad (2)$$

where $f_k(\boldsymbol{\Theta},t)(k=1,2,\cdots,n_{\mathrm{d}})$ is the nonlinear restoring force of the kth energy-dissipation device.

Using the first passage failure criterion with symmetric double boundary value, the seismic reliability of the energy-dissipation structure described in Eq. (1) can be defined as

$$P_{\mathrm{r}}=\mathrm{P}\{|s(\boldsymbol{\Theta},t)|\le b,\ t\in[0,T]\} \quad (3)$$

where $\mathrm{P}\{\bullet\}$ indicates the probability of the random event; T is the duration of the seismic excitation; b is the value of the symmetric boundary; and $s(\boldsymbol{\Theta},t)$ is the critical response that controls the structural failure.

The expression of Eq. (3) is equivalent to

$$P_{\mathrm{r}}=\mathrm{P}\{Z(\boldsymbol{\Theta},T)\le b\} \quad (4)$$

where

$$Z(\boldsymbol{\Theta},T)=\max_{t\in[0,T]}|s(\boldsymbol{\Theta},t)| \quad (5)$$

is the peak absolute value of the critical response $s(\boldsymbol{\Theta},t)$ over time interval $[0,T]$. Assume that the PDF of the peak response $Z(\boldsymbol{\Theta},T)$ has been obtained. Then, based on Eq. (4), the seismic reliability of the energy-dissipation structure can be directly evaluated as

$$P_{\mathrm{r}}=\int_0^b p_Z(z)\mathrm{d}z \quad (6)$$

where $p_Z(z)$ is the peak-response PDF. Hence, the failure probability of the energy-dissipation structure is $P_{\mathrm{f}}=1-P_{\mathrm{r}}$.

2.2. Evaluation of peak-response PDF by PDEM

The PDEM can be used to obtain the peak-response PDF $p_Z(z)$ by constructing a virtual random process as follows:

$$Y(\tau)=Z(\boldsymbol{\Theta},T)\cdot\tau \quad (7)$$

where τ is the virtual time. It can be seen from Eq. (7) that the peak response $Z(\boldsymbol{\Theta},T)$ equals the value of the virtual random process $Y(\tau)$ at the time instant $\tau=1$, i.e.

$$Z(\boldsymbol{\Theta},T)=Y(\tau)\big|_{\tau=1} \tag{8}$$

Once the evolutionary PDF of the virtual random process $Y(\tau)$, $p_Y(y,\tau)$, is obtained, one can immediately get the peak-response PDF as

$$p_Z(z)=p_Y(y,\tau)\big|_{\tau=1,\ y=z} \tag{9}$$

Employing the thoughts of PDEM and noting that $\dot{Y}(\tau)=Z(\boldsymbol{\Theta},T)$ from Eq. (7), the probability density evolution equation with regard to the joint PDF of $(Y(\tau),\boldsymbol{\Theta})$ can be obtained as

$$\frac{\partial p_{Y\boldsymbol{\Theta}}(y,\boldsymbol{\theta},\tau)}{\partial\tau}+Z(\boldsymbol{\theta},T)\frac{\partial p_{Y\boldsymbol{\Theta}}(y,\boldsymbol{\theta},\tau)}{\partial y}=0 \tag{10}$$

with the initial condition

$$p_{Y\boldsymbol{\Theta}}(y,\boldsymbol{\theta},\tau)\big|_{\tau=0}=\delta(y)\,p_{\boldsymbol{\Theta}}(\boldsymbol{\theta}) \tag{11}$$

where $\delta(\bullet)$ is the Dirac function and $p_{\boldsymbol{\Theta}}(\boldsymbol{\theta})$ is the joint PDF of the random vector $\boldsymbol{\Theta}$.

Solving the initial-value problem (10) and (11) for $p_{Y\boldsymbol{\Theta}}(y,\boldsymbol{\theta},\tau)$, one can obtain the evolutionary PDF of $Y(\tau)$ as the marginal distribution of $p_{Y\boldsymbol{\Theta}}(y,\boldsymbol{\theta},\tau)$, i.e.

$$p_Y(y,\tau)=\int_{\Omega_{\boldsymbol{\Theta}}}p_{Y\boldsymbol{\Theta}}(y,\boldsymbol{\theta},\tau)\mathrm{d}\boldsymbol{\theta} \tag{12}$$

where $\Omega_{\boldsymbol{\Theta}}$ is the distribution domain of $\boldsymbol{\Theta}$. Then, the peak-response PDF $p_Z(z)$ can be obtained using Eqs. (9) and (12).

To solve Eq. (10), $\boldsymbol{\theta}$ must be first prescribed and the peak response $Z(\boldsymbol{\theta},T)$, i.e. the value of the coefficient in Eq. (10), should then be determined through numerical integration of the nonlinear equation of motion (1). After that Eq. (10) can be solved numerically and the integral with regard to $\boldsymbol{\theta}$ in Eq. (12) can be carried out eventually.

It should be noted that, for each representative point $\boldsymbol{\theta}$, one needs to conduct one nonlinear time-history analysis of the energy-dissipation structure shown in Eq. (1), and there could be hundreds of representative points to ensure the accuracy of the numerical integration in Eq. (12). Therefore, hundreds of nonlinear time-history analyses would be embedded in the solution process of PDEM, which leads to relatively high computational cost for large-scale engineering structures when conventional numerical integration methods are adopted. To enhance the efficiency of PDEM, the ETDM with dimension-reduced explicit iteration scheme can be used to conduct the high-efficient nonlinear time-history analyses of the energy-dissipation structure, which will be elaborated in Section 3 that follows.

3. NONLINEAR TIME-HISTORY ANALYSIS OF ENERGY-DISSIPATION STRUCTURES BY ETDM

3.1. Time-domain explicit expressions of dynamic responses

Substituting a prescribed representative point $\boldsymbol{\Theta}=\boldsymbol{\theta}$ into Eq. (1), one can derive a deterministic nonlinear equation of motion as

$$\mathbf{M}\ddot{\mathbf{U}}+\mathbf{C}\dot{\mathbf{U}}+\mathbf{K}\mathbf{U}+\mathbf{L}_{\mathrm{D}}\mathbf{F}_{\mathrm{D}}(\boldsymbol{\theta},\mathbf{V}_{\mathrm{D}})=-\mathbf{M}\mathbf{E}X(\boldsymbol{\theta},t) \tag{13}$$

Moving the nonlinear term $\mathbf{L}_{\mathrm{D}}\mathbf{F}_{\mathrm{D}}(\boldsymbol{\theta},\mathbf{V}_{\mathrm{D}})$ to the right-hand side of Eq. (13), one can obtain the following quasi-linear equation of motion as

$$\mathbf{M}\ddot{\mathbf{U}}+\mathbf{C}\dot{\mathbf{U}}+\mathbf{K}\mathbf{U}=\mathbf{L}\mathbf{F}(\boldsymbol{\theta},\mathbf{V}_{\mathrm{D}},t) \tag{14}$$

where

$$\mathbf{F}(\boldsymbol{\theta},\mathbf{V}_{\mathrm{D}},t)=[X(\boldsymbol{\theta},t)\ \ \mathbf{F}_{\mathrm{D}}^{\mathrm{T}}(\boldsymbol{\theta},\mathbf{V}_{\mathrm{D}})]^{\mathrm{T}} \tag{15}$$

and

$$\mathbf{L}=-[\mathbf{M}\mathbf{E}\ \ \mathbf{L}_{\mathrm{D}}] \tag{16}$$

are the equivalent excitation vector and the corresponding orientation matrix, respectively.

For the quasi-linear equation of motion shown in Eq. (14), define the state vector as $\mathbf{V}=[\mathbf{U}^{\mathrm{T}}\ \ \dot{\mathbf{U}}^{\mathrm{T}}]^{\mathrm{T}}$. Then, the recurrence formula for the state vector can be written as

$$\mathbf{V}_i=\mathbf{T}\mathbf{V}_{i-1}+\mathbf{Q}_1\mathbf{F}_{i-1}(\boldsymbol{\theta},\mathbf{V}_{\mathrm{D},i-1})+\mathbf{Q}_2\mathbf{F}_i(\boldsymbol{\theta},\mathbf{V}_{\mathrm{D},i})\quad(i=1,2,\cdots,n) \tag{17}$$

where $n = T/\Delta t$ is the number of time steps for time-history analysis with Δt being the time step; the subscripts i and $i-1$ denote $t_i = i\Delta t$ and $t_{i-1} = (i-1)\Delta t$, respectively; and $\mathbf{T}$, $\mathbf{Q}_1$ and $\mathbf{Q}_2$ can be deduced based on the Newmark-β integration scheme, which can be expressed as (Su et al., 2016)

$$\begin{cases} \mathbf{T} = \begin{bmatrix} \mathbf{H}_{11} & \mathbf{H}_{12} \\ \mathbf{H}_{21} & \mathbf{H}_{22} \end{bmatrix},\ \mathbf{Q}_1 = \begin{bmatrix} \mathbf{R}_1 \\ \mathbf{R}_3 \end{bmatrix}\mathbf{L},\ \mathbf{Q}_2 = \begin{bmatrix} \mathbf{R}_2 \\ \mathbf{R}_4 \end{bmatrix}\mathbf{L} \\ \mathbf{H}_{11} = \hat{\mathbf{K}}^{-1}(\mathbf{S}_1 - \mathbf{S}_3\mathbf{M}^{-1}\mathbf{K}) \\ \mathbf{H}_{12} = \hat{\mathbf{K}}^{-1}(\mathbf{S}_2 - \mathbf{S}_3\mathbf{M}^{-1}\mathbf{C}) \\ \mathbf{H}_{21} = a_3(\mathbf{H}_{11} - \mathbf{I}) + a_5\mathbf{M}^{-1}\mathbf{K} \\ \mathbf{H}_{22} = a_3\mathbf{H}_{12} - a_4\mathbf{I} + a_5\mathbf{M}^{-1}\mathbf{C} \\ \mathbf{R}_1 = \hat{\mathbf{K}}^{-1}\mathbf{S}_3\mathbf{M}^{-1},\ \mathbf{R}_2 = \hat{\mathbf{K}}^{-1} \\ \mathbf{R}_3 = a_3\mathbf{R}_1 - a_5\mathbf{M}^{-1},\ \mathbf{R}_4 = a_3\mathbf{R}_2 \\ \hat{\mathbf{K}} = \mathbf{K} + a_0\mathbf{M} + a_3\mathbf{C} \\ \mathbf{S}_1 = a_0\mathbf{M} + a_3\mathbf{C},\ \mathbf{S}_2 = a_1\mathbf{M} + a_4\mathbf{C},\ \mathbf{S}_3 = a_2\mathbf{M} + a_5\mathbf{C} \\ a_0 = \dfrac{1}{\beta\Delta t^2},\ a_1 = \dfrac{1}{\beta\Delta t},\ a_2 = \dfrac{1}{2\beta} - 1 \\ a_3 = \dfrac{\gamma}{\beta\Delta t},\ a_4 = \dfrac{\gamma}{\beta} - 1,\ a_5 = \dfrac{\Delta t}{2}\left(\dfrac{\gamma}{\beta} - 2\right) \end{cases} \tag{18}$$

where $\mathbf{I}$ is the unit matrix, and γ and β are two parameters related to the integration stability. In this study, $\gamma = 0.5$ and $\beta = 0.25$ are used and the Newmark-β integration scheme will be unconditionally stable.

Assuming $\mathbf{V}_0 = \mathbf{0}$, based on Eq. (17), one can derive the explicit expression of the state vector at each time instant as

$$\begin{aligned} \mathbf{V}_i = {} & \mathbf{A}_{i,0}\mathbf{F}_0(\boldsymbol{\theta}, \mathbf{V}_{\mathrm{D},0}) + \mathbf{A}_{i,1}\mathbf{F}_1(\boldsymbol{\theta}, \mathbf{V}_{\mathrm{D},1}) + \cdots \\ & + \mathbf{A}_{i,i-1}\mathbf{F}_{i-1}(\boldsymbol{\theta}, \mathbf{V}_{\mathrm{D},i-1}) + \mathbf{A}_{i,i}\mathbf{F}_i(\boldsymbol{\theta}, \mathbf{V}_{\mathrm{D},i}) \\ & (i = 1, 2, \cdots, n) \end{aligned} \tag{19}$$

where $\mathbf{F}_j(\boldsymbol{\theta}, \mathbf{V}_{\mathrm{D},j})(j = 0, 1, \cdots, i)$ are the equivalent excitation vectors at different time instants, and $\mathbf{A}_{i,0}, \mathbf{A}_{i,1}, \cdots, \mathbf{A}_{i,i}$ are the corresponding coefficient matrices, which are only associated with $\mathbf{M}$, $\mathbf{C}$, $\mathbf{K}$ and $\mathbf{L}$ in Eq. (14) and can be expressed in closed forms as

$$\begin{cases} \mathbf{A}_{1,0} = \mathbf{Q}_1,\ \mathbf{A}_{i,0} = \mathbf{T}\mathbf{A}_{i-1,0} \quad (2 \le i \le n) \\ \mathbf{A}_{1,1} = \mathbf{Q}_2,\ \mathbf{A}_{2,1} = \mathbf{T}\mathbf{Q}_2 + \mathbf{Q}_1,\ \mathbf{A}_{i,1} = \mathbf{T}\mathbf{A}_{i-1,1} \quad (3 \le i \le n) \\ \mathbf{A}_{i,j} = \mathbf{A}_{i-1,j-1} \quad (2 \le j \le i \le n) \end{cases} \tag{20}$$

It can be observed from Eq. (20) that only the coefficient matrices $\mathbf{A}_{i,0}$ and $\mathbf{A}_{i,1}$ $(i = 1, 2, \cdots, n)$ need to be determined and stored, while the other coefficient matrices can be directly obtained from $\mathbf{A}_{i,1}(i = 1, 2, \cdots, n)$.

3.2. Dimension-reduced explicit iteration scheme

With the advantage of explicit representation of the state vector, $\mathbf{V}_i$ in Eq. (19) can be divided into two vectors. The first vector is $\mathbf{V}_{\mathrm{D},i}$, which consists of the nodal displacements and velocities directly associated with the nonlinear restoring forces of the energy-dissipation devices, and the other vector can be denoted as $\mathbf{V}_{\mathrm{R},i}$, which is composed of the rest components of $\mathbf{V}_i$ except for those in $\mathbf{V}_{\mathrm{D},i}$. Correspondingly, Eq. (19) can be divided into two equations as follows:

$$\begin{aligned} \mathbf{V}_{\mathrm{D},i} = {} & \mathbf{A}^{\mathrm{D}}_{i,0}\mathbf{F}_0(\boldsymbol{\theta}, \mathbf{V}_{\mathrm{D},0}) + \mathbf{A}^{\mathrm{D}}_{i,1}\mathbf{F}_1(\boldsymbol{\theta}, \mathbf{V}_{\mathrm{D},1}) + \cdots \\ & + \mathbf{A}^{\mathrm{D}}_{i,i-1}\mathbf{F}_{i-1}(\boldsymbol{\theta}, \mathbf{V}_{\mathrm{D},i-1}) + \mathbf{A}^{\mathrm{D}}_{i,i}\mathbf{F}_i(\boldsymbol{\theta}, \mathbf{V}_{\mathrm{D},i}) \\ & (i = 1, 2, \cdots, n) \end{aligned} \tag{21}$$

$$\begin{aligned} \mathbf{V}_{\mathrm{R},i} = {} & \mathbf{A}^{\mathrm{R}}_{i,0}\mathbf{F}_0(\boldsymbol{\theta}, \mathbf{V}_{\mathrm{D},0}) + \mathbf{A}^{\mathrm{R}}_{i,1}\mathbf{F}_1(\boldsymbol{\theta}, \mathbf{V}_{\mathrm{D},1}) + \cdots \\ & + \mathbf{A}^{\mathrm{R}}_{i,i-1}\mathbf{F}_{i-1}(\boldsymbol{\theta}, \mathbf{V}_{\mathrm{D},i-1}) + \mathbf{A}^{\mathrm{R}}_{i,i}\mathbf{F}_i(\boldsymbol{\theta}, \mathbf{V}_{\mathrm{D},i}) \\ & (i = 1, 2, \cdots, n) \end{aligned} \tag{22}$$

where $\mathbf{A}^{\mathrm{D}}_{i,j}$ and $\mathbf{A}^{\mathrm{R}}_{i,j}$ consist of the rows simply extracted from $\mathbf{A}_{i,j}(j = 0, 1, \cdots, i)$ with respect to $\mathbf{V}_{\mathrm{D},i}$ and $\mathbf{V}_{\mathrm{R},i}$, respectively.

It can be observed from Eqs. (21) and (22) that the nonlinear iteration can be carried out just focusing on $\mathbf{V}_{\mathrm{D},i}$ via Eq. (21). Once $\mathbf{V}_{\mathrm{D},i}$ is obtained, the other responses in $\mathbf{V}_{\mathrm{R},i}$ can be directly calculated using Eq. (22) without any further iteration. In general, only a limit number of energy-dissipation devices are used in an energy-dissipation structure. Therefore, Eq. (21)

is only a small-size system of nonlinear algebraic equations, which will lead to much higher efficiency for nonlinear analysis. Note that the above dimension-reduced explicit iteration scheme can yield the results of responses at the same accuracy as those obtained with the traditional nonlinear time-history analysis methods because no truncation treatment is introduced in the present scheme.

In practical engineering design, not all structural responses are required, and only a certain number of critical responses need to be acquired. Therefore, with the explicit expression of $\mathbf{V}_{\mathrm{R},i}$ in Eq. (22), one can also conduct the dimension-reduced calculation of the responses in $\mathbf{V}_{\mathrm{R},i}$, which will further enhance the efficiency of the subsequent response analysis. Suppose s_i is a critical response component in $\mathbf{V}_{\mathrm{R},i}$. Then, from Eq. (22), s_i can be directly obtained as

$$\begin{aligned} s_i = {} & \mathbf{a}_{i,0}^{s}\mathbf{F}_0(\boldsymbol{\theta},\mathbf{V}_{\mathrm{D},0}) + \mathbf{a}_{i,1}^{s}\mathbf{F}_1(\boldsymbol{\theta},\mathbf{V}_{\mathrm{D},1}) + \cdots \\ & + \mathbf{a}_{i,i-1}^{s}\mathbf{F}_{i-1}(\boldsymbol{\theta},\mathbf{V}_{\mathrm{D},i-1}) + \mathbf{a}_{i,i}^{s}\mathbf{F}_i(\boldsymbol{\theta},\mathbf{V}_{\mathrm{D},i}) \quad (23) \\ & (i=1,2,\cdots,n) \end{aligned}$$

where $\mathbf{a}_{i,j}^{s}$ is the corresponding row vector of $\mathbf{A}_{i,j}^{\mathrm{R}}(j=0,1,\cdots,i)$ with respect to s_i.

In summary, using the time-domain explicit expressions of dynamic responses shown in Eq. (19), dimension-reduced analysis can be easily conducted with high efficiency for time-history analysis of the energy-dissipation structure equipped with nonlinear energy-dissipation devices. The analysis procedure is composed of two steps. The first step is the dimension-reduced iteration for the nodal displacements and velocities of energy-dissipation devices using Eq. (21), and the second step is the dimension-reduced calculation of the other critical responses using Eq. (23).

4. SOLUTION PROCESS OF PDEM-ETDM

As can be seen from Section 3, the ETDM with dimension-reduced explicit iteration scheme can be incorporated into PDEM to conduct high-efficient nonlinear time-history analyses of the energy-dissipation structure. This hybrid approach, which combines the thoughts of PDEM and ETDM, can be termed as PDEM-ETDM. For the sake of clarity, the solution procedures of PDEM-ETDM for seismic reliability analysis of energy-dissipation structures are summarized as follows:

(1) Select representative points $\boldsymbol{\theta}_q(q=1,2,\cdots,N)$ in the distribution domain $\Omega_{\boldsymbol{\Theta}}$, where N is the total number of the selected points. The strategy of selecting points can be found in Li and Chen (2007).

(2) Calculate the matrices $\mathbf{T}$, $\mathbf{Q}_1$ and $\mathbf{Q}_2$ using Eq. (18) and determine the coefficient matrices $\mathbf{A}_{i,j}(i=1,2,\cdots,n;\ j=0,1,\cdots,i)$ using Eq. (20). Then extract $\mathbf{A}_{i,j}^{\mathrm{D}}$ shown in Eq. (21) from $\mathbf{A}_{i,j}$ with respect to $\mathbf{V}_{\mathrm{D},i}$, and extract $\mathbf{a}_{i,j}^{s}$ shown in Eq. (23) from $\mathbf{A}_{i,j}$ with respect to any critical response s_i.

(3) For a prescribed representative point $\boldsymbol{\theta}_q$, conduct the nonlinear dimension-reduced iteration focusing on $\mathbf{V}_{\mathrm{D},i}$ through Eq. (21), and then carry out the dimension-reduced calculation for any critical response s_i using Eq. (23). Start from $i=1$ and repeat this step until $i=n$.

(4) Calculate the peak response $Z(\boldsymbol{\theta}_q,T)$ using Eq. (5) based on the obtained $s_i(i=1,2,\cdots,n)$, and then solve the initial-value problem (10) and (11) for $p_{Y\boldsymbol{\Theta}}(y,\boldsymbol{\theta}_q,\tau)$ with the finite difference method. The details for implementation of the finite difference method can be found in Li and Chen (2009).

(5) Repeat steps (3) and (4) for each representative point until all points have been considered.

(6) Carry out the numerical integration with regard to $\boldsymbol{\theta}$ in Eq. (12) based on the obtained $p_{Y\boldsymbol{\Theta}}(y,\boldsymbol{\theta}_q,\tau)(q=1,2,\cdots,N)$ to evaluate the evolutionary PDF $p_Y(y,\tau)$.

(7) Determine the peak-response PDF $p_Z(z)$ using Eq. (9) from $p_Y(y,\tau)$, and then evaluate the seismic reliability of the energy-dissipation structure using Eq. (6).

It can be seen from the above procedures that the coefficient matrices required for construction of the time-domain explicit expressions of dynamic responses need to be calculated only once and can be used for all the selected points, and owing to the use of explicit formulation of dynamic responses, dimension-reduced analysis can be easily conducted for each selected point. These merits lead to a significant reduction in computational cost for PDEM.

5. ENGINEERING APPLICATION

5.1. The suspension bridge

A 2,040 m long suspension bridge now being built in South China, as shown in Figure 1, is used to illustrate the accuracy and efficiency of the proposed approach for seismic reliability analysis of large-scale energy-dissipation structures. The bridge has a main span of 1,200 m, leading to a rise-span ratio of 1:9.5. Each main tower of the bridge has 2 cross beams and rises to a level of 191 m. To restrain the excessive longitudinal displacement of the main girder under seismic excitations, the suspension bridge is equipped with 4 nonlinear fluid viscous dampers, as illustrated in Figure 2. The viscous dampers are installed between the lower cross beam of the main tower and the bottom plate of the main girder. The nonlinear damping force-velocity relation for viscous dampers can be analytically expressed as a fractional velocity power law

$$f(t) = \text{sign}(v) C_{\text{D}} |v|^{\alpha} \tag{24}$$

where $f(t)$ is the damping force of the viscous damper; sign(•) is the sign function; v is the axial nodal relative velocity between damper ends; and C_{D} and α are the damping coefficient and the velocity exponent of the viscous damper, respectively, which are mutually independent random variables with the probabilistic information listed in Table 1. In this study, the damper parameters are assumed to be the same for all viscous dampers, and two cases are considered for different coefficients of variation of the damper parameters.

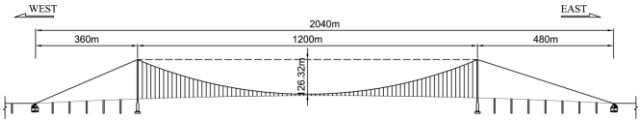

Figure 1: Elevation of a suspension bridge.

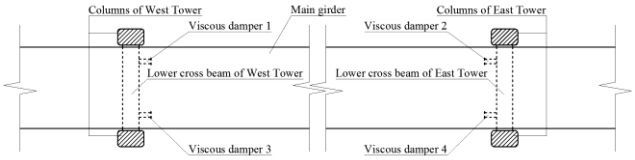

Figure 2: Locations of viscous dampers between main tower and main girder.

Table 1: Probabilistic information of the random parameters.

Random variable	*Distribution type*	*Case 1*		*Case 2*	
		Mean	*COV*	*Mean*	*COV*
C_{D} (kN/(m·s^{-1})$^{\alpha}$)	*Normal*	*2,500*	*0.1*	*2,500*	*0.2*
α	*Normal*	*0.4*	*0.1*	*0.4*	*0.2*
ζ_1 (m/s^2)	*Normal*	*2.0*	*0.25*	*2.0*	*0.25*
ζ_2 (m/s^2)	*Normal*	*2.0*	*0.25*	*2.0*	*0.25*

Note: COV = coefficient of variation.

5.2. Finite element model

The finite element model of the suspension bridge is established using the general-purpose finite element software ANSYS, as shown in Figure 3. The whole model consists of 479 beam elements and 374 truss elements, leading to a total number of 5,100 degrees of freedom for the whole structure. The completion state of the suspension bridge is obtained through form-finding analysis, in which geometric nonlinear effects, including the large-displacement and stress-stiffening effects under the dead load of the bridge, are taken into consideration. It has been observed that the newly induced geometric nonlinear effects due to seismic excitations can be neglected as compared with those induced by the dead load of the bridge during erection. Therefore, the above model can be used to

conduct the subsequent seismic reliability analysis of the suspension bridge after completion.

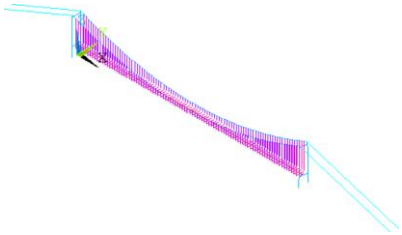

Figure 3: Finite element model of suspension bridge after completion.

5.3. Random seismic excitation

The ground motion acceleration is assumed to be random combination of two time histories (Li and Chen, 2007), i.e.

$$\ddot{x}_g(t) = \zeta_1 \ddot{x}_{g_1}(t) + \zeta_2 \ddot{x}_{g_2}(t) \tag{25}$$

where $\ddot{x}_{g_1}(t)$ and $\ddot{x}_{g_2}(t)$ are the standardized N-S and E-W El-Centro records with the unit amplitude, respectively, and ζ_1 and ζ_2 are mutually independent random variables with the probabilistic information also listed in Table 1.

5.4. Seismic reliability analysis

The first passage failure criterion with symmetric double boundary value is used for this engineering application, and the critical response that controls the structural failure is taken as the longitudinal displacement at mid-span of the main girder. Seismic reliability analysis of the suspension bridge equipped with nonlinear viscous dampers is conducted using the PDEM-ETDM presented in Section 4. To demonstrate the accuracy and efficiency of the proposed approach, seismic reliability analysis is also carried out using Monte Carlo simulation (MCS) with $N_s = 10^5$ samples. In the above two methods, the duration of the time-history analysis is set to be $T = 30$ s with the time step being $\Delta t = 0.02$ s . The total number of the selected representative points for PDEM-ETDM is $N_p = 864$.

The curves of failure probability of the suspension bridge corresponding to the two cases are shown in Figure 4 and Figure 5, respectively. It can be seen that the results obtained by PDEM-ETDM are in good agreement with those obtained by MCS for all levels of thresholds, demonstrating the good accuracy of the proposed approach.

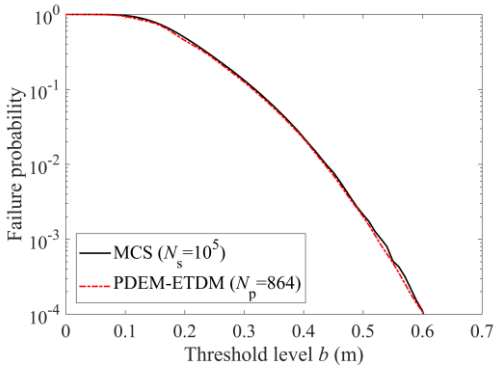

Figure 4: Curve of failure probability (Case 1).

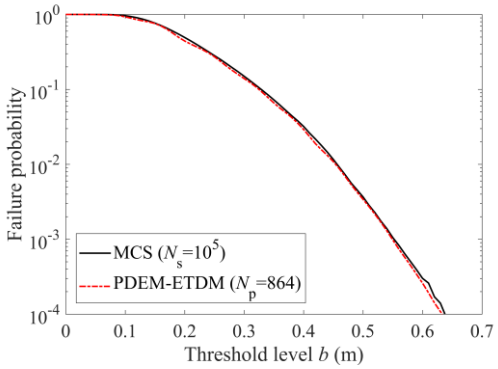

Figure 5: Curve of failure probability (Case 2).

The structural failure probabilities with respect to different thresholds corresponding to the two different cases are presented in Table 2 and Table 3, respectively. From the tables it can be seen that the failure probabilities computed by the PDEM-ETDM is of fair accuracy. It can be further observed that, at the same level of threshold, the failure probability of the structure increases with the increase of the coefficients of variation of the damper parameters. At a low threshold level, e.g. $b = 0.28$ m , the increase rate of the failure probability is small. However, on the contrary, at a high threshold level, e.g. $b = 0.58$ m , the increase rate of the failure probability could be large, which indicates that, for the case of small failure probability, it is necessary to take into account the influence due to the uncertainties of the damper parameters

besides the effect due to the random seismic excitation.

Table 2: Failure probability of the structure (Case 1).

Method	*Threshold level b* (m)			
	0.28	*0.38*	*0.48*	*0.58*
PDEM-ETDM	*0.17*	*0.032*	*0.0033*	*0.00019*
MCS	*0.18*	*0.034*	*0.0035*	*0.00022*

Table 3: Failure probability of the structure (Case 2).

Method	*Threshold level b* (m)			
	0.28	*0.38*	*0.48*	*0.58*
PDEM-ETDM	*0.18*	*0.042*	*0.0053*	*0.00044*
MCS	*0.19*	*0.045*	*0.0056*	*0.00050*

As for the computational efficiency, it can be seen from Figure 4 and Figure 5 that the number of nonlinear dynamic analyses required by PDEM is much smaller than that required by MCS. Take Case 2 for further illustration. The time elapsed by PDEM-ETDM is just 1,567 s (26.1 min), while the time elapsed by the PDEM in conjunction with the traditional nonlinear analysis method (TNAM), which can be termed as PDEM-TNAM, is up to 746,496 s (8.64 d), as presented in Table 4. The high efficiency of the present approach is owing to the fact that the average time spent on each nonlinear time-history analysis by ETDM is only 1.8 s, while that by TNAM is around 864 s (14.4 min). For seismic reliability analysis of such a large-scale engineering problem involving nonlinear structural behaviors, the elapsed time of less than 30 minutes is relatively short and can be accepted in practical application, indicating the feasibility of the proposed approach.

Table 4: Comparison of elapsed time by different seismic reliability analysis methods (Case 2).

Method	*Elapsed time* (s)
PDEM-ETDM	*1,567*
PDEM-TNAM	*746,496*

6. CONCLUSIONS

A hybrid approach, termed as PDEM-ETDM, has been proposed for seismic reliability analysis of large-scale energy-dissipation structures with uncertain parameters of nonlinear energy-dissipation devices subjected to random seismic excitations. The ETDM with dimension-reduced iteration scheme is used to conduct the high-efficient nonlinear time-history analyses embedded in the solution process of PDEM, which leads to a significant reduction of computational cost for PDEM. The proposed approach is successfully applied to the seismic reliability analysis of a suspension bridge with nonlinear viscous dampers, indicating the feasibility of the proposed approach to engineering problems.

7. ACKNOWLEDGEMENTS

The research is funded by the National Natural Science Foundation of China (51678252) and the Science and Technology Program of Guangzhou, China (201804020069).

8. REFERENCES

Chen, J. B., and Li, J. (2007). "The extreme value distribution and dynamic reliability analysis of nonlinear structures with uncertain parameters" *Structural Safety*, 29, 77–93.

Li, J., and Chen, J. B. (2007). "The number theoretical method in response analysis of nonlinear stochastic structures" *Computational Mechanics*, 39(6), 693–708.

Li, J., and Chen, J. B. (2009). *Stochastic Dynamics of Structures*, New York: John Wiley & Sons.

Soong, T. T., and Spencer, B. F. (2002). "Supplemental energy dissipation: state-of-the-art and state-of-the-practice" *Engineering Structures*, 24(3), 243–259.

Su, C., Huang, H., and Ma, H. T. (2016). "Fast equivalent linearization method for nonlinear structures under nonstationary random excitations" *Journal of Engineering Mechanics*, 142(8), 4016049.

Su, C., Li, B. M., Chen, T. C., and Dai, X. H. (2018a). "Stochastic optimal design of nonlinear viscous dampers for large-scale structures subjected to non-stationary seismic excitations based on dimension-reduced explicit method" *Engineering Structures*, 175, 217–230.

Su, C., Liu, X. L., Li, B. M., and Huang, Z. J. (2018b). "Inelastic response analysis of bridges subjected to non-stationary seismic excitations by efficient MCS based on explicit time-domain method" *Nonlinear Dynamics*, DOI: 10.1007/s11071-018-4477-6.